FEBS Letters 505 (2001) 18–22 FEBS 25171

Crystal structure of neuroserpin: a neuronal serpin involved in a conformational disease

Christophe Briand, Serguei V. Kozlov, Peter Sonderegger, Markus G. Grütter*

Institute of Biochemistry, University of Zürich, Winterthurerstrasse 190, CH-8057 Zürich, Switzerland

Received 12 June 2001; revised 30 July 2001; accepted 30 July 2001

First published online 17 August 2001

Edited by Hans Eklund

Abstract The protease inhibitor neuroserpin regulates the development of the nervous system and its plasticity in the adult. Neuroserpins carrying the Ser53Pro or Ser56Arg mutation form polymers in neuronal cells. We describe here the structure of wild-type neuroserpin in a cleaved form. The structure provides a basis to understand the role of the mutations in the polymerization process. We propose that these mutations could delay the insertion of the reactive center loop into the central β-sheet A, an essential step in the inhibition and possibly in the polymerization of neuroserpin.

Key words: Serpin; Protease inhibitor; Crystal structure; Polymerization

1. Introduction

Neuroserpin is a serine protease inhibitor belonging to the serpin family [1,2]. It is expressed in neurons of the central and peripheral nervous system in the adult and during development [3]. Complex formation and inhibition assays have demonstrated that it is a potent inhibitor of tissue-type plasminogen activator (tPA), urokinase plasminogen activator and plasmin. In contrast, no inhibition of thrombin activity was observed [4,5]. Studies of the interactions between neuroserpin and its target proteases indicate that it acts, like other serpins, as a suicide inhibitor by forming an extremely stable acyl complex with its target proteases. Inhibition involves cleavage of the reactive center loop (RCL) between residues P1 and P1′ [6], and insertion of its N-terminal portion into β-sheet A. We have determined the structure of neuroserpin in its cleaved form. Our crystallographic results indicate that residues P1 and P1′ are separated by 70 Å (Fig. 1), as it was observed in the structure of human α1-proteinase inhibitor [7]. RCL insertion into β-sheet A critically depends on a sliding mechanism: β-strand s3A, belonging to β-sheet A, slides over the so-called shutter region [8], that is the end of β-strand s6B and the beginning of α-helix hB (blue in Fig. 1, see also legend). Mutations in the shutter region affect RCL insertion and impair the inhibition mechanism (for a review, see [9]). In some cases, such mutations lead to the formation of serpin polymers [9]. Recently, two point mutants of neuroserpin (Ser53Pro and Ser56Arg, nomenclature defined by Loebermann et al. [7]) were discovered in two families suffering from presenile dementia. In both families, the affected individuals underwent progressive neuronal degeneration due to the formation of inclusion bodies composed of polymerized uncleaved mutant neuroserpin in the cerebral cortex [10]. Both point mutants belong to the shutter region.

Based on our crystal structure, we discuss the possible effect of the two mutants associated with pathogenic polymerization. We propose that the two mutations could affect the rate of loop insertion.

2. Materials and methods

2.1. Expression and purification of mouse neuroserpin (mNS)

The construct used for expressing homogenous neuroserpin in *Escherichia coli* was designed with a deletion of the last 13 amino acids at the C-terminus. Using the mNS cDNA encoding amino acids 17–410 cloned in the pAK400 vector [11] via the *Nde*I and *Hin*dIII sites without the pelB leader as a template [3], a polymerase chain reaction (PCR) was performed with Pfu polymerase (Stratagene) according to the manufacturer's protocol. The amplification was performed with the primer pair 5′-ag**catatg**acagggcaacgttcccagatg-3′ (*Nde*I site is underlined) and 5′-tc**aagcTT**ATTA*atggtgatggtgatgat*gagggttcatgactcgtcccatg-3′ (*Hin*dIII site is underlined, His-tag sequence is indicated in italics, two *ochre*-stop codons are capitalized). The resulting PCR product was verified by sequencing of both strands, digested with *Nde*I and *Hin*dIII and ligated into the pAK400 vector. Expression and purification were performed as described by Krueger et al. [3]. A hydrophobic interaction chromatography was included. After adding ammonium sulfate to obtain a final concentration of 1.5 M, the protein solution was loaded onto a HP phenyl Sepharose XK16 (Pharmacia©) column. The protein was eluted using a gradient from 900 mM to 0 mM ammonium sulfate in PS buffer (200 mM Tris–HCl pH 8.0, 50 mM NaCl) over 10 column volumes. Fractions containing the pure, uncleaved protein were pooled and dialyzed against a storage buffer (10 mM Tris–HCl pH 8.0, 50 mM NaCl).

2.2. Complex formation assay and amidolytic assay

Complex formation assays and amidolytic assays were performed as described by Krueger et al. [3] with recombinant human tPA (Genentech, South San Francisco, CA, USA) and human thrombin (Sigma, St. Louis, MO, USA).

2.3. Crystallization, data collection and processing

Prior to crystallization, mNS was cleaved with 1:3 of trypsin from bovine pancreas (Fluka, 93608) overnight at 4°C in 50 mM Tris–HCl pH 8.4, 200 mM NaCl, 0.3 mM $CaCl_2$. The protein was then purified with a MonoQ HR10/10 column (Pharmacia©) using a buffer contain-

*Corresponding author. Fax: (41)-1-635 68 34.
E-mail address: gruetter@bioc.unizh.ch (M.G. Grütter).

Abbreviations: mNS, mouse neuroserpin; mNSd13C, mouse neuroserpin with a deletion of 13 C-terminal residues; NCS, non-crystallographic symmetry; PCR, polymerase chain reaction; PDB, Protein Data Bank; RCL, reactive center loop; tPA, tissue-type plasminogen activator

PII: S0014-5793(01)02764-8

ing 20 mM Tris–HCl pH 8.0, 0.1 mM phenylmethylsulfonyl fluoride and a gradient from 200 mM to 400 mM NaCl on 40 column volumes. Fractions containing the pure cleaved protein were pooled, concentrated to 25 mg/ml using a Centricon YM-10 (Amicon, Millipore) and buffer was exchanged with the storage buffer. A single crystal was used for data collection. It was grown over 1 week at 20°C from a sitting drop of 1:1 mixture of the protein sample and a reservoir solution containing 25% PEG_{8000}, 0.2 M $H_2PO_4(NH_4)$, 0.1 M Tris–HCl pH 6.1. The crystal exhibited initial diffraction to 2.7 Å resolution. The space group was found to be $P2_1$ ($a=64.3$ Å, $b=108.7$ Å, $c=46.0$ Å, $\beta=101.3°$). A dataset was collected at 100 K with a 300 mm Mar Research Image plate using CuKα radiation (Nonius generator FR571 operating at 45 kV, 95 mA), focused by a double mirror system from Prophysics (XRM-216). The data (see Table 1) were processed with Denzo and scaled with Scalepack [12].

2.4. Structure determination and refinement

The structure was solved by molecular replacement using the program AmoRe [13] and a polyserine consensus model, based on 10 cleaved serpin structures [7,14–18], generated using Modeller [19]. Using the data from 10 Å to 4 Å, AmoRe indicated the presence of two molecules in the asymmetric unit related by a non-crystallographic symmetry (NCS) axis. Both translation solutions had an *R*-value of 47.1% and a correlation coefficient of 38.1%. The solvent content was determined to be 30% [20]. Density modification (solvent flattening, histogram matching and 2-fold averaging) with DM [21] yielded phases of sufficient quality to build a model of neuroserpin containing most side chains. The program O was used for this purpose [22]. After rigid-body refinement with CNS [23], torsion angle simulated annealing was performed with 2-fold NCS constraints (CNS). A bulk solvent correction (17–3.06 Å) was applied as well as an anisotropy correction (8–3.06 Å). Additional cycles of rebuilding and refinement, followed by an individual *B*-factor refinement, yielded a crystallographic *R*-value of 23.2% and an R_{free} of 30.8%. The atomic coordinates have been deposited with the Brookhaven Protein Data Bank (PDB; code 1JJO).

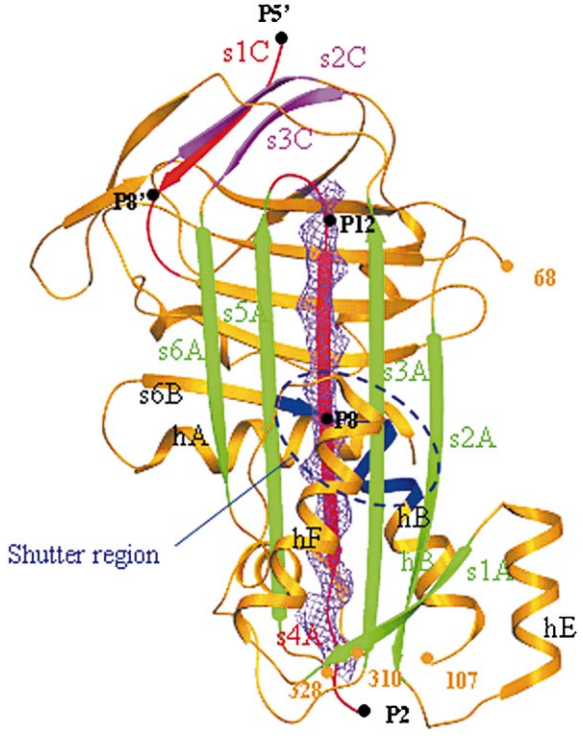

Fig. 1. Ribbon diagram of mNSd13C. Secondary structure elements are labeled according to Loebermann et al. [7]. The 'shutter region' is colored in blue [8]. The RCL (in red) is inserted after cleavage into the β-sheet A (in green) to form the β-strand s4A. The RCL also forms the β-strand s1C of the β-sheet C (in purple). A $2F_o-F_c$ electron density map (1σ contour) shows the presence of the β-strand s4A.

Table 1
Crystallographic data

Cell parameters (space group $P2_1$)	
a (Å)	64.3
b (Å)	108.7
c (Å)	46.0
α (°)	90.0
β (°)	101.3
γ (°)	90.0
No. molecules per asymmetric unit	2
Data collection	
Resolution limits (Å)	17.00–3.06
No. unique reflections	9419 (7975)[a]
Redundancy	2.57
Completeness (%)	79.7 (74.6)[b]
Average I/σ	5.8 (2.0)[b]
$R_{sym}(I)$[c] (%)	15.5 (42.2)[b]
Refinement	
R^{d}_{factor} (%)	23.2
R^{e}_{free} (%)	30.8
Rmsd bonds (Å)	0.008
Rmsd angles (°)	1.42

[a] $>2\sigma$.
[b] Statistics for the highest resolution shell (3.14–3.06 Å).
[c] $R_{sym}(I)=\Sigma_{hkl}\Sigma_j|I_{j,hkl}-\langle I_{hkl}\rangle|/\Sigma_{hkl}\Sigma_{j,hkl}$, where $\langle I_{hkl}\rangle$ is the average of the intensity $I_{j,hkl}$ over $j=1$, ..., N observations of symmetry equivalent reflections *hkl*.
[d] $R_{factor}=\Sigma||F_o|-|F_c||/\Sigma|F_o|$, where $|F_o|$ and $|F_c|$ are observed and scaled calculated structure factor amplitudes respectively. The R_{factor} is calculated on 8914 reflections (75.5%).
[e] 4.3% of the data (505 reflections).

3. Results and discussion

3.1. Crystallization and activity tests of recombinant neuroserpin

Sequence alignment with other previously crystallized serpins reveals that mNS possesses 13 additional residues at the C-terminus. We cloned neuroserpin in a bacterial expression system without those 13 residues to avoid a possible tail that could create structural heterogeneities, hampering crystallization. The C-terminally truncated form (mNSd13C) was tested in vitro for activity and was found to be as active as wild-type mNS prepared as described by Krueger et al. [3] (Fig. 2A). The ability of mNSd13C and mNS to inhibit the amidolytic activity of tPA and thrombin on a chromogenic substrate (D-isoleucyl-L-propyl-L-arginine-*p*-nitroaniline-dihydrochloride, Chromogenix, Mölndal, Sweden) was also compared (Fig. 2B). The inhibition level of mNSd13C was the same as previously observed by Krueger et al. for mNS [3].

Various attempts to crystallize uncleaved mNSd13C were not successful, possibly the flexibility of the RCL prevents the regular arrangement of the molecule into a crystal lattice. We therefore tried to crystallize a cleaved form of mNSd13C. Trypsin digestion was used to produce a cleaved species that crystallized.

3.2. Structure description

The structure of the cleaved form of mNSd13C reveals a cleaved RCL and a deletion of a segment comprising residues 69–106 (α-helices hC, hD and connecting loop). The topology of neuroserpin (Fig. 1) is identical to that of other cleaved serpin structures [7,14–18,24]. Although marked sequence differences exist between different serpins, structural differences

are only seen in loop regions, resulting mainly from the variable loop lengths. Compared to the first cleaved α1-antiproteinase structure [7], mNSd13C contains the following additional residues: 179A to 179B, 235A to 235F, 246A, 258A. A complete insertion of the RCL into β-sheet A to form β-strand s4A is observed. As expected for a functional inhibitor, mNSd13C cleaved by trypsin shows the expected relaxed serpin form and not the stressed form of plakalbumin [25] where the RCL is cleaved but not inserted. The loop comprising residues 311–327 (before β-strand s5A) is not visible in the structure, but its presence was proven by matrix-assisted laser desorption ionization mass spectrometry performed on protein from dissolved crystals. Similarly, a part of the corresponding loop in the crystal structure of antithrombin (PDB code 1AHT, residues B356–B361) [26] was also missing, indicating flexibility in this region. Likewise, no electron density was found for residues P1 and P1′ to P4′.

3.3. *Model building and role of residues Ser53 and Ser56 during the insertion of the RCL*

Using the crystal structures of mNSd13C (present work), α1-antitrypsin [27], plasminogen activator inhibitor 2 [28] and preinserted antithrombin as templates [26], models of the native and preinserted forms of neuroserpin were created. Ser53-Pro and Ser56Arg models were also created. The hydrogen

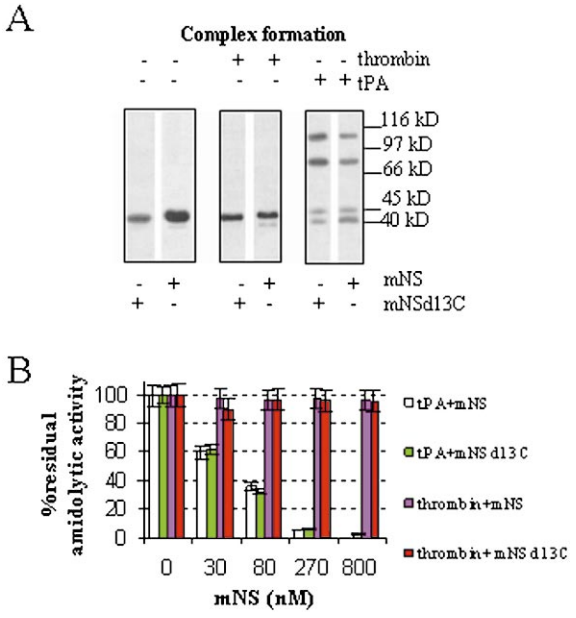

Fig. 2. Activity tests. A: Analysis of the complex formation of mNS and of C-terminally truncated neuroserpin (mNSd13C) with tPA and thrombin. Since neuroserpin forms sodium dodecyl sulfate-stable complexes with tPA but not with thrombin [4,5], 5 μM mNS or mNSd13C was incubated with 5 μM of tPA or thrombin. Neuroserpin or neuroserpin-containing complexes were detected by Western blot. For both mNS and mNSd13C, two complexes with tPA were found with an apparent molecular weight (MW) that corresponds to the sum of the MW of the neuroserpin and of a single-chain tPA or a double-chain tPA. In contrast, no thrombin-containing complex was observed. The possible cross-reactivity of the antiserum with tPA was first checked and found to be negative (data not shown). B: mNS and mNSd13C similarly inhibit the amidolytic activity of tPA but fail to inhibit thrombin. tPA or thrombin (8 nM) were preincubated with various concentrations of both neuroserpins. The protease substrate D-isoleucyl-L-prolyl-L-arginine-*p*-nitroaniline was added and *p*-nitroaniline release was measured.

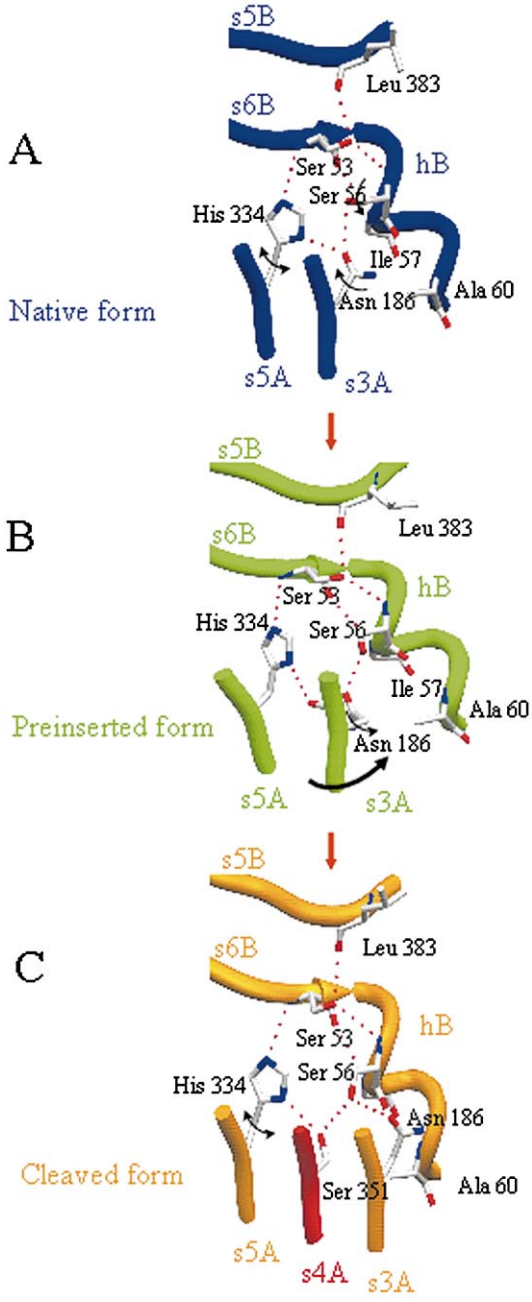

Fig. 3. Ser53 and Ser56 and the insertion of RCL: a model. A: The 'shutter region' in the native form (in dark blue, template α1-antitrypsin [27]). A ring of hydrogen bonds links the side chain of Ser56, His334 and Asn186. B: After preinsertion of the RCL (in green), His334 must rotate and interact with the backbone C=O of Asn186. During the preinsertion of the RCL, Val188 slides between Ser53 and Ser56 (Fig. 4A), so Ser56 must also rotate. Consequently, Asn186 has to rotate to maintain its interaction with Ser56 (antithrombin structure used as a template [26]). C: Asn186 continues to slide between residues 56 and 60 (Fig. 4A). Its side chain rotates to a similar position as seen in the native form. Ser351 takes the place of Asn186 and the β-strand s3A translocates from its preinserted position to its relaxed position (in orange; structure of neuroserpin). The loss of the hydrogen bond between Asn186 and His334 is compensated for by the formation of a hydrogen bond with the OH side chain of Ser351. Prepared with Setor [31].

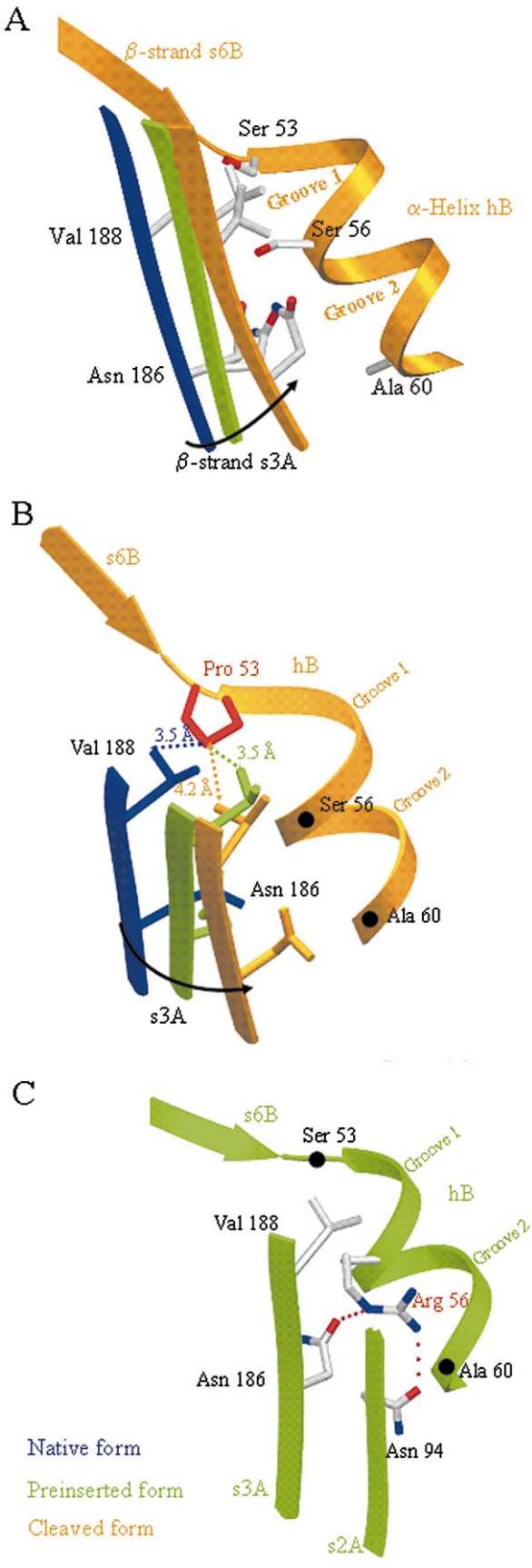

Fig. 4. Effect of the two mutations on the RCL insertion mechanism. A: During the preinsertion (β-strand s3A in blue moved to the position in green) and the full insertion of the RCL (β-strand s3A in orange) Val188 has to slide into groove 1 of α-helix hB (residues 53–56). Likewise, Asn186 has to slide into groove 2 of α-helix hB (residues 56–60). B: Effect of the Ser53Pro mutation. β-Strand s6A and α-helix hB of the cleaved form are colored in orange. By adding a new hydrophobic residue in the native form (in dark blue) and in the preinserted form (in green), Val188 of β-strand s3A can make a hydrophobic interaction with Pro53. After RCL insertion, a rearrangement in the bottom part of β-strand s3A occurs, affecting the position of Val188. Since this hydrophobic interaction must be disrupted after preinsertion to fully insert the RCL, the rate of insertion could be reduced. C: Effect of the Ser56Arg mutation. Arg56 replaces Ser56, which normally swings during the insertion of the reactive loop [28]. Conversely, in the native form and in the preinserted form (here in green) the Nε side chain of Arg56 can hydrogen-bond the Oδ side chain of Asn186. The Nη1 or Nη2 side chain of Arg56 will also hydrogen-bond the Oδ side chain of Asn94. Arg56 is at the place where Asn186 has to slide when the loop is fully inserted. To fully insert the RCL, Arg56 must lose its hydrogen bonds and shift into another position, that is also slowing down the rate of the full insertion. Prepared with Setor [31].
←

bonding pattern of the shutter region was analyzed in the models of native and preinserted neuroserpin, and in the crystal structure (cleaved form) (Fig. 3A–C). This analysis suggests that Ser53 should maintain its structurally important interactions in all three forms without any rotation of its side chain during the transition from the native to the fully inserted form. In contrast, Ser56 (Fig. 3A–C) has to rotate during this transition [28]. On the other hand, Val188 has to slide between Ser53 and Ser56 (Fig. 4A). Mutations of Ser53 or Ser56 could affect the sliding of Val188 and then impair the full insertion of the RCL. Analysis of Ser53Pro and Ser56Arg models suggests that these two point mutations could lead to a decrease in the rate of conversion of the preinserted form to the relaxed (latent or cleaved) form (Fig. 4B,C). A preinserted form of neuroserpin would therefore be accumulated in the mutants and could be the reason for their tendency to polymerize. We hypothesize that polymerization could occur by insertion of the RCL of one preinserted molecule into the bottom part of the central β-sheet A of a second molecule. This mechanism is in accordance with previous proposals of polymer models [27,29,30]. In order to prove experimentally the role of mutations Ser53Pro and Ser56Arg we will prepare the mutant molecules and analyze the effect of the mutations on the aggregation behavior. This experiment will be carried out on both cleaved and native mNS.

Acknowledgements: We would like to thank Stephan Krueger, Guido Capitani, Ragna Sack and Mrudula Donepudi. This work was supported by the Baugartenstiftung (CH-8022 Zürich). C.B. was supported by a grant from l'Association pour la Recherche contre le Cancer.

References

[1] Osterwalder, T., Contartese, J., Stoeckli, E.T., Kuhn, T.B. and Sonderegger, P. (1996) EMBO J. 15, 2944–2953.
[2] Schrimpf, S.P., Bleiker, A.J., Brecevic, L., Kozlov, S.V., Berger, P., Osterwalder, T., Krueger, S.R., Schinzel, A. and Sonderegger, P. (1997) Genomics 40, 55–62.
[3] Krueger, S.R., Ghisu, G.P., Cinelli, P., Gschwend, T.P., Osterwalder, T., Wolfer, D.P. and Sonderegger, P. (1997) J. Neurosci. 17, 8984–8996.

[4] Hastings, G.A., Coleman, T.A., Haudenschild, C.C., Stefansson, S., Smith, E.P., Barthlow, R., Cherry, S., Sandkvist, M. and Lawrence, D.A. (1997) J. Biol. Chem. 272, 33062–33067.
[5] Osterwalder, T., Cinelli, P., Baici, A., Pennella, A., Krueger, S.R., Schrimpf, S.P., Meins, M. and Sonderegger, P. (1998) J. Biol. Chem. 273, 2312–2321.
[6] Schechter, I. and Berger, A. (1967) Biochem. Biophys. Res. Commun. 27, 157–162.
[7] Loebermann, H., Tokuoka, R., Deisenhofer, J. and Huber, R. (1984) J. Mol. Biol. 177, 531–557.
[8] Stein, P.E., Leslie, A.G., Finch, J.T. and Carrell, R.W. (1991) J. Mol. Biol. 221, 941–959.
[9] Stein, P.E. and Carrell, R.W. (1995) Nat. Struct. Biol. 2, 96–113.
[10] Davis, R.L., Shrimpton, A.E., Holohan, P.D., Bradshaw, C., Felglin, D., Collins, H.G., Sonderegger, P., Kinter, J., Becker, L.M., Lacbawan, F., Krasnewich, D., Muenke, M., Lawrence, D.A., Yerby, M.S., Shaw, C.-M., Gooptu, B., Elliott, P.R., Finch, J.T., Carrell, R.W. and Lomas, D.A. (1999) Nature 401, 376–379.
[11] Krebber, A., Bornhauser, S., Burmester, J., Honegger, A., Willuda, J., Bosshard, H.R. and Pluckthun, A. (1997) J. Immunol. Methods 201, 35–55.
[12] Otwinowski, Z. and Minor, W. (1996) in: Methods in Enzymology (Abelson, J.N. and Simon, M.I., Eds.), Vol. 276, pp. 307–326, Academic Press, New York.
[13] Navaza, J. (1994) Acta Crystallogr. A50, 157–163.
[14] Lukacs, C.M., Zhong, J.Q., Plotnick, M.I., Rubin, H., Cooperman, B.S. and Christianson, D.W. (1996) Nat. Struct. Biol. 3, 888–893.
[15] Mourey, L., Samama, J.P., Delarue, M., Petitou, M., Choay, J. and Moras, D. (1993) J. Mol. Biol. 232, 223–241.
[16] Baumann, U., Bode, W., Huber, R., Travis, J. and Potempa, J. (1992) J. Mol. Biol. 226, 1207–1218.
[17] Baumann, U., Huber, R., Bode, W., Grosse, D., Lesjak, M. and Laurell, C.B. (1991) J. Mol. Biol. 218, 595–606.
[18] Engh, R., Lobermann, H., Schneider, M., Wiegand, G., Huber, R. and Laurell, C.B. (1989) Protein Eng. 2, 407–415.
[19] Sali, A., Potterton, L., Yuan, F., Vlijmen, H.v. and Karplus, M. (1995) Proteins 23, 318–326.
[20] Matthews, B. (1968) J. Mol. Biol. 33, 491–497.
[21] CCP4 (1994) Acta Crystallogr. D50, 760–763.
[22] Jones, T., Zou, J.N. and Kjeldgaard, M. (1991) Acta Crystallogr. A47, 110–119.
[23] Brünger, A., Adams, P., Clore, G., DeLano, W., Gros, P., Grosse-Kunstleve, R., Jiang, J., Kuszewski, J., Nilges, M., Pannu, N., Read, R., Rice, L., Simonson, T. and Warren, G. (1998) Acta Crystallogr. D54, 905–921.
[24] Sussman, J., Lin, D., Jiang, J., Manning, N., Prilusky, J., Ritter, O. and Abola, E. (1998) Acta Crystallogr. D54, 1078–1084.
[25] Wright, H.T., Qian, H.X. and Huber, R. (1990) J. Mol. Biol. 213, 513–528.
[26] Schreuder, H.A., de Boer, B., Dijkema, R., Mulders, J., Theunissen, H.J., Grootenhuis, P.D. and Hol, W.G. (1994) Nat. Struct. Biol. 1, 48–54.
[27] Elliott, P.R., Lomas, D.A., Carrell, R.W. and Abrahams, J.P. (1996) Nat. Struct. Biol. 3, 676–681.
[28] Harrop, S.J., Jankova, L., Coles, M., Jardine, D., Whittaker, J.S., Gould, A.R., Meister, A., King, G.C., Mabbutt, B.C. and Curmi, P.M. (1999) Struct. Fold Des. 7, 43–54.
[29] Carrell, R.W. and Gooptu, B. (1998) Curr. Opin. Struct. Biol. 8, 799–809.
[30] Mahadeva, R., Chang, W.S., Dafforn, T.R., Oakley, D.J., Foreman, R.C., Calvin, J., Wight, D.G. and Lomas, D.A. (1999) J. Clin. Invest. 103, 999–1006.
[31] Evans, S.V. (1993) J. Mol. Graph. 11, 134–138.